Supporting Information

Cobalt Macrocyclic Complexes-Catalyzed Selective Electroreduction of CO_2 to CO

Wen-Jun Xie,[a] Jin-Mei Chen,[a] Zhi-Wen Yang,[a] and Liang-Nian He*[a,b]

[a]State Key Laboratory and Institute of Elemento-Organic Chemistry, Frontiers Science Center for New Organic Matter, College of Chemistry, Nankai University, Tianjin 300071, China

[b]Carbon Neutrality Interdisciplinary Science Centre, Nankai University, Tianjin 300350, China

*Corresponding Author
E-mail Addresses: heln@nankai.edu.cn (L.-N. He)

Table of Contents

1. Materials and reagents

Carbon dioxide (purity 99.999%) and Ar (purity 99.999%) were used. Pyrrole was distilled before use. The $KHCO_3$ solution used for ECO_2RR has been pretreated with Chelex 100 resin before electrolysis to get rid of other potential trace metal ions and keep away from impurity metal deposition. Purified multi-walled carbon nanotubes (MWCNT or CNT, Macklin, inner diameter: 5-10 nm; outer diameter: 10-20 nm; length: 10-30 μm) were treated by 5 wt% HCl aqueous solution. The carbon paper (CDS180S) was sonicated for 8 h in 1 M nitric acid aqueous solution, water and acetone successively. The N117 proton exchange membranes were heated at 80 °C in 5 wt% H_2O_2 aqueous solution, water, 1M H_2SO_4 and water successively. Unless otherwise stated, other materials and reagents were purchased from commercial sources and used without further treatment.

2. Instrumentation and characterizations

^1H NMR and $^{13}C\{^1H\}$ NMR spectra were recorded on AVANCE III HD 400 spectrometer with residual solvent peaks used as the internal reference. High resolution mass spectrometry (HRMS) analysis was performed on Varian 7.0T spectrometer by electrospray ionization (ESI) technique or Bruker Solarix scimax spectrometer by matrix assisted laser desorption ionization (MALDI) technique. Fourier transform infrared (FT-IR) spectra were recorded on a Bruker Tensor 27 FT-IR spectrophotometer with KBr pellets. Ultraviolet visible spectrophotometer (UV-vis) absorption spectra were measured on an Agilent Cary 60 spectrophotometer at room temperature. X-ray photoelectron spectroscopy (XPS) data were collected on Thermo SCIENTIFIC ESCALAB Xi+ under ultrahigh vacuum (< 10^{-9} mbar) using a monochromatic Al Kα X-ray source. Raman spectra data were collected on Horiba scientific-LabRAM HR evolution. Scanning electron microscopy (SEM) was characterized on ZEISS SIGMA 500 with Bruker 60 dual probe energy dispersive spectrometer (EDS). The metal contents of the catalysts were analyzed using inductively coupled plasma-optical emission spectrometry (ICP-OES) on SpectroBlue. All the electrochemical tests were performed with CHI 660D electrochemical workstation. Analysis of gas product was conducted on gas chromatograph FULI 9790 equipped with thermal conductivity detector (TCD) using Ar as carrier gas.

3. Catalysts synthesis and electrode preparation

Synthesis of 5-phenyldipyrromethane. The procedure is according to the literature with some modification.[1] Benzaldehyde (2132.7 mg, 20.1 mmol), pyrrole (140.0 mL, 2.0 mol) and $InCl_3$ (444.2 mg, 2.0 mmol) were stirred at room temperature under Ar for 6 h. Then 4 g NaOH was added to quench the reaction for 45 min to afford an orange red solution. The mixture was centrifuged and the supernatant was evaporated under vacuum to remove the pyrrole. Then the greyish yellow solid was washed with hexane and evaporated to remove the traces of pyrrole. Subsequently, the product was purified by silica gel column chromatography (petroleum ether/CH_2Cl_2/ethyl acetate = 7/2/1, V/V/V) to give a pale yellow solid 1634.5 mg (yield 36.5%). ^1H NMR (400 MHz, DMSO-d_6): δ (ppm) 10.55 (s, 2H), 7.30-7.11 (m, 5H), 6.60 (d, J = 1.8 Hz, 2H), 5.89 (d, J = 2.7 Hz, 2H), 5.65 (s, 2H), 5.34 (s, 1H). $^{13}C\{^1H\}$ NMR (101 MHz, $CDCl_3$): δ (ppm) 142.20, 132.64, 128.76, 128.52, 127.10, 117.36, 108.52, 107.34, 44.08. m.p. 102-103 °C.

Synthesis of 5-phenyl-α,α'-dibromodipyrrin. The procedure is according to the literature with some modification.[2] 5-phenyldipyrromethane (333.4 mg, 1.5 mmol) in 22.5 mL dry tetrahydrofuran (THF) was cooled to -78 °C under Ar. N-Bromosuccinimide (NBS) (533.9 mg, 3 mmol) was added to the solution in three portions every 15 min and stirred for 1 h. Then 1,2-Dichloro-4,5-Dicyanobenzoquinone (DDQ) (340.5 mg, 1.5 mmol) was added and the mixture was stirred at -78 °C for 10 min and at room temperature for 20 min to afford a dark red solution. The mixture was first subjected to a short alumina column (CH_2Cl_2) and the purified by silica gel column chromatography (petroleum ether/ethyl acetate = 4/1, V/V) to give an orange solid 456.3 mg (yield 79.3%). ^1H NMR (400 MHz, $CDCl_3$) δ (ppm) 7.51-7.41 (m, 5H), 6.48 (d, J = 4.1 Hz, 2H), 6.34 (d, J = 4.3 Hz, 2H). $^{13}C\{^1H\}$ NMR (101 MHz, $CDCl_3$) δ (ppm) 140.43, 139.53, 135.54, 130.87, 130.34, 129.66, 129.49, 127.97, 120.56. m.p. 161-162 °C.

Synthesis of 5,15-diaza-10,20-diphenylporphyrin (H_2DAP). The procedure is according to the literature with some modification.[3] 5-phenyl-α,α'-dibromodipyrrin (760.0 mg, 2 mmol), $Pb(acac)_2$ (407.8 mg, 1 mmol), Bu_4NI (1479.0 mg, 4 mmol) and NaN_3 (264.6 mg, 4 mmol) in 300 mL 1-propanol were stirred at 100 °C under Ar for 47 h. Then the solution was concentrated to 100 mL and washed with toluene and water. The organic phase was purified by silica gel column chromatography (CH_2Cl_2/ethyl acetate = 95/5, V/V) to afford a purple solid. In order to remove the Pd^{2+}, TFA (1.0 mL, 13.1 mmol) and 70 mL CH_2Cl_2 were added and the solution was stirred at 0 °C for 1 h. The mixture was purified by silica gel column chromatography (CH_2Cl_2/ethyl acetate = 95/5, V/V) to afford a purple solid 62.2 mg (yield 26.8%). ^1H NMR (400 MHz, $CDCl_3$): δ (ppm) 9.33 (d, J = 4.8 Hz, 4H), 9.05 (d, J = 4.8 Hz, 4H), 8.25-8.14 (m, 4H), 7.89-7.77 (m, 6H), -2.75 (s, 2H). $^{13}C\{^1H\}$ NMR (101 MHz, $CDCl_3$): δ (ppm) 122.68, 127.37, 128.51, 132.65, 133.78, 134.92, 139.38, 148.24, 153.62. HRMS (ESI) Calcd. for $C_{30}H_{21}N_6$ $[M + H]^+$: 465.1828 Found: 465.1825. UV/Vis (DMF): λ_{max} (ε) = 395 nm (452000), 506 nm (25100), 543 nm (83400), 576 nm (23300), 627 nm (104000 M^{-1} cm^{-1}). IR (KBr, cm^{-1}): υ_{max} = 3274 cm^{-1} (N-H), δ_{max} = 945 cm^{-1} (N-H).

Synthesis of cobalt 5,15-diazaporphyrin (CoDAP). The procedure is according to the literature with some modification.[4] 5,15-diaza-10,20-diphenylporphyrin (62.2 mg, 0.13 mmol) and $Co(OAc)_2$ (231.7 mg, 1.3 mmol) in 13 mL 1,2-dichlorobenzene were stirred at 110 °C under Ar for 17 h. The mixture was purified by silica gel column chromatography (CH_2Cl_2/ethyl acetate = 95/5, V/V) to afford a dark purple solid 59.5 mg (yield 87.8%). ^1H NMR (400 MHz, $CDCl_3$) δ (ppm) 13.48 (br), 11.76 (br), 9.58 (br), 9.39 (br). HRMS (MALDI)

Calcd. for $CoC_{30}H_{19}N_6$ $[M + H]^+$: 522.1003 Found: 522.0991. UV/Vis (DMF): λ_{max} (ε) = 366 nm (142000), 397 nm (160000), 566 nm (117000 M^{-1} cm^{-1}).

Synthesis of catalyst/CNT hybrid materials. The procedure is according to the literature with some modification.[5] 60.0 mg MWCNT in 50 mL DMF was sonicated for 1 h to disperse the MWCNT. Then 5.0 mg CoDAP was dissolved in 10 mL DMF. The above solutions were mixed and sonicated for 0.5 h, which were then stirred at room temperature for 14 h. The suspension was centrifuged and the black precipitate was washed with DMF and water. Finally, the solid was lyophilized to yield the final product 41.4 mg. The weight percentage of cobalt in the CoDAP/CNT was measured as 0.344 wt% by ICP-OES test.

DAP/CNT, CoPc/CNT and CoTPP/CNT were synthesized by the same way and the weight percentage of cobalt was measured as 0.000 wt%, 0.519 wt% and 0.013 wt%, respectively.

Preparation of working electrode. To prepare the CoDAP/CNT/CP: 2.0 mg CoDAP/CNT was added into a mixture of 60 μL 0.5 wt% Nafion solution and 1940 μL ethanol. The suspension was sonicated for 1 h. 400 μL catalyst ink was drop-coated on an 1×1 cm^{-2} cabon paper, which was heated at ~75 °C to evaporate the ethanol.

CoPc/CNT/CP, DAP/CNT/CP and CNT/CP was prepared by the same way.

To prepare the CoTPP@CNT/CP: 200μL CoTPP solution (3.1 mg CoTPP with 2 mL DMF) was added into a mixture of 240 μL 0.5 wt% Nafion solution, 1960 μL DMF and 8.0 mg MWCNT. The suspension was sonicated for 2 h. 120 μL catalyst ink was drop-coated on an 1×1 cm^{-2} cabon paper, which was heated at ~100 °C to evaporate the DMF.

4. Electrochemical measurements

Electrochemical measurements were performed by using CHI 660D electrochemical working station and a commercial gas-tight two-compartment cell (Fig. S22†). The two compartments of the cell were separated by N117 proton exchange membrane. Three-electrode system was used. Graphite rod and Ag/AgCl/KCl (sat.) electrode were used as counter electrode and reference electrode, respectively. The as-prepared working electrode was held by a glass carbon electrode holder. The electrolyte was 0.1 M $KHCO_3$ and the volume in one compartment was 20.0 mL. Before electrochemical measurements, Ar or CO_2 was bubbled for 25 min to saturate the cathodic electrolyte and then the compartment was sealed with the volume of head space was approximately 48.7 mL. The potentials in linear sweep voltammetry (LSV) and constant potential electrolysis (CPE) tests were *i*R corrected at 90% level. And all the potentials values versus RHE were calculated by the equation (the pH values of CO_2 and Ar saturated 0.1 M $KHCO_3$ were 6.8 and 8.2, respectively):

$$E\ (V\ vs\ RHE) = E\ (V\ vsAg/AgCl)\ + 0.197 + 0.0592\ \times\ pH$$

The surface concentration (Γ) of electroactive metal sites were determined by cyclic voltammetry (CV) at various scan rate (20, 40, 60, 80, 100 mV/s) and were calculated by the equation:

$$I_p = \frac{n^2F^2S\Gamma v}{4RT}$$

I_p is the peak current of the Co(II)/Co(I) reduction wave, n is the number of transferred electrons (1 e^-), S is the geometric surface area of the working electrode (1 cm^{-2}), F is Faraday's constant, R is the gas constant, T is the temperature, and v is the scan rate.

5. Products analysis

After CPE tests, gas from the head of cathodic compartment was drawn by a gas-tight syringes and injected in the gas chromatography, which equipped with a thermal conductivity detector (TCD) and could analyze the volume of gas product qualitatively and quantitatively. The volume of generated H_2 or CO was calculated by calibration curves (Fig. S23†). The liquid product (MeOH) was analyzed by ^1H NMR with DMSO as the internal standard (Fig. S24†).

Faradaic efficiency (FE) was calculated as following:

$$FE = \frac{nNF}{Q}\ \times\ 100\%$$

n is the moles of product; N is the moles of electrons for obtaining per mole product; F is the Faradaic constant (96485 C mol^{-1}); Q is the charge flowing through the electrode surface (C).

For gas product, n (mol) was calculated as following:

$$n = \frac{PV}{RT}$$

P, V, R, and T represent the atmospheric pressure (101000 Pa), gas volume (m^3), gas constant (8.314 J mol^{-1} K^{-1}) and room temperature (298 K), respectively.

Electroactive turnover frequency (eTOF) was calculated as following:

$$eTOF = \frac{n}{\Gamma_{Co}t}$$

Γ_{Co} is the electroactive Co loading calculated by CV measurements; t is the time of CPE (3600 s).

6. DFT calculation details

Theoretical calculations were performed on the basis of density functional theory (DFT), as implemented in the GAUSSIAN 09 packages (G09) and the Vienna ab initio simulation packages (VASP).

For G09, all the calculated Mulliken charge populations were taken from optimized structures, which were performed at the B3LYP hybrid functional level[6, 7] using the pseudopotential LANL2DZ basis set on transition metal Co atom and the 6-311+G(d,p) basis set on all the other (H, C, and N) atoms. All calculations used the polarizable continuum model (PCM) to model solvent effects (water).[8] Dispersion correction was conducted by DFT-D3.[7]

For VASP, the first-principles[9, 10] was employed to perform all density functional theory (DFT) calculations within the generalized gradient approximation (GGA) using the Perdew-Burke-Ernzerhof (PBE)[11] formulation. The projected augmented wave (PAW) potentials[12, 13] was chosen to describe the ionic cores and take valence electrons into account using a plane wave basis set with a kinetic energy cutoff of 520 eV. Partial occupancies of the Kohn−Sham orbitals were allowed using the Gaussian smearing method with a width of 0.02 eV. The electronic energy was considered self-consistent when the energy change was smaller than 10^{-6} eV. A geometry optimization was considered convergent when the energy change was smaller than 0.03 eV $Å^{-1}$. In addition, for the Co atoms, the U schemes need to be applied, and the U has been set as 4.21 eV. The vacuum spacing in a direction perpendicular to the plane of the structure is 18 Å for the structures. The Brillouin zone integration is performed using 2×2×1 Monkhorst-Pack k-point sampling for a structure. Finally, the adsorption energies (Eads) were calculated as Eads= Ead/sub -Ead -Esub, where Ead/sub, Ead, and Esub are the total energies of the optimized adsorbate/substrate system, the adsorbate in the structure, and the clean substrate, respectively. The free energy was calculated using the equation:

$$G = E + ZPE - TS$$

where G, E, ZPE and TS are the free energy, total energy from DFT calculations, zero point energy and entropic contributions, respectively. For the calculation of adsorption state frequency, the high K-point density (4×4×1 Monkhorst-Pack k-point) calculation had been used.

7. Synthesis route and products characterization charts

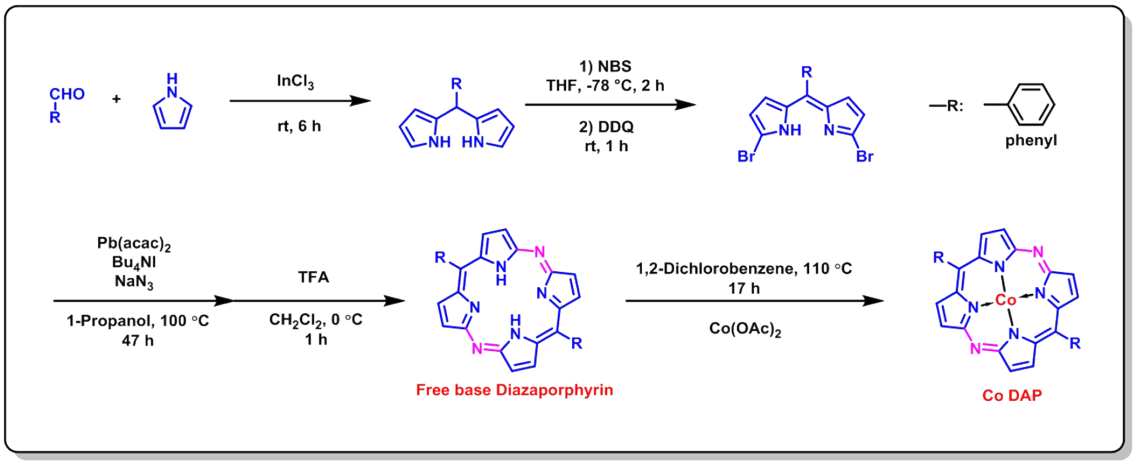

Fig. S1 Synthesis route to Co 5,15- diazaporphyrin.

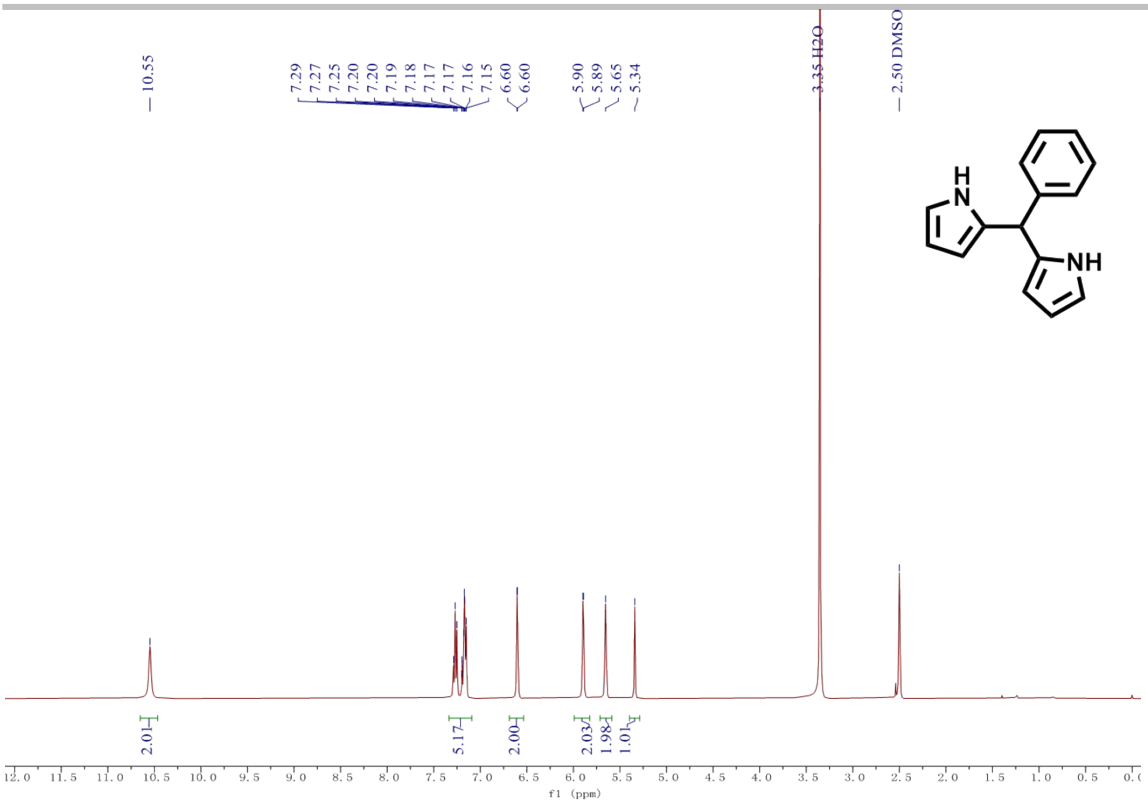

Fig. S2 ^{1}H NMR chart of 5-phenyldipyrromethane (400 MHz, DMSO-d_6).

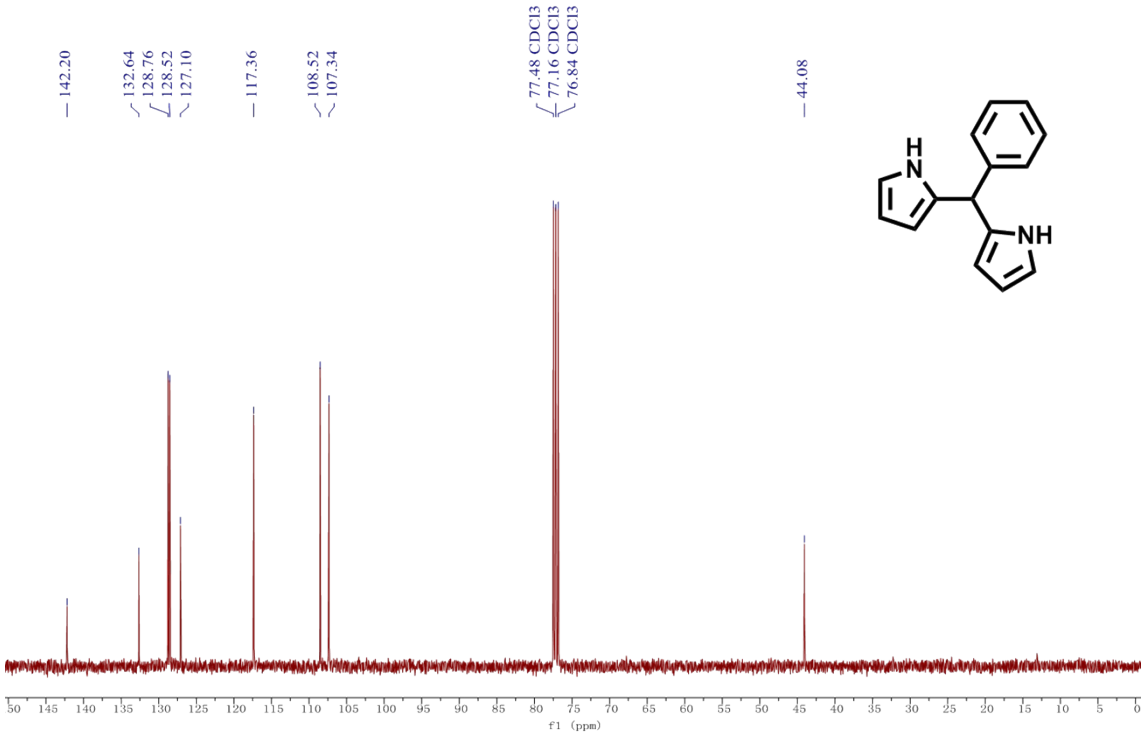

Fig. S3 ^{13}C{^{1}H} NMR chart of 5-phenyldipyrromethane (101 MHz, $CDCl_3$).

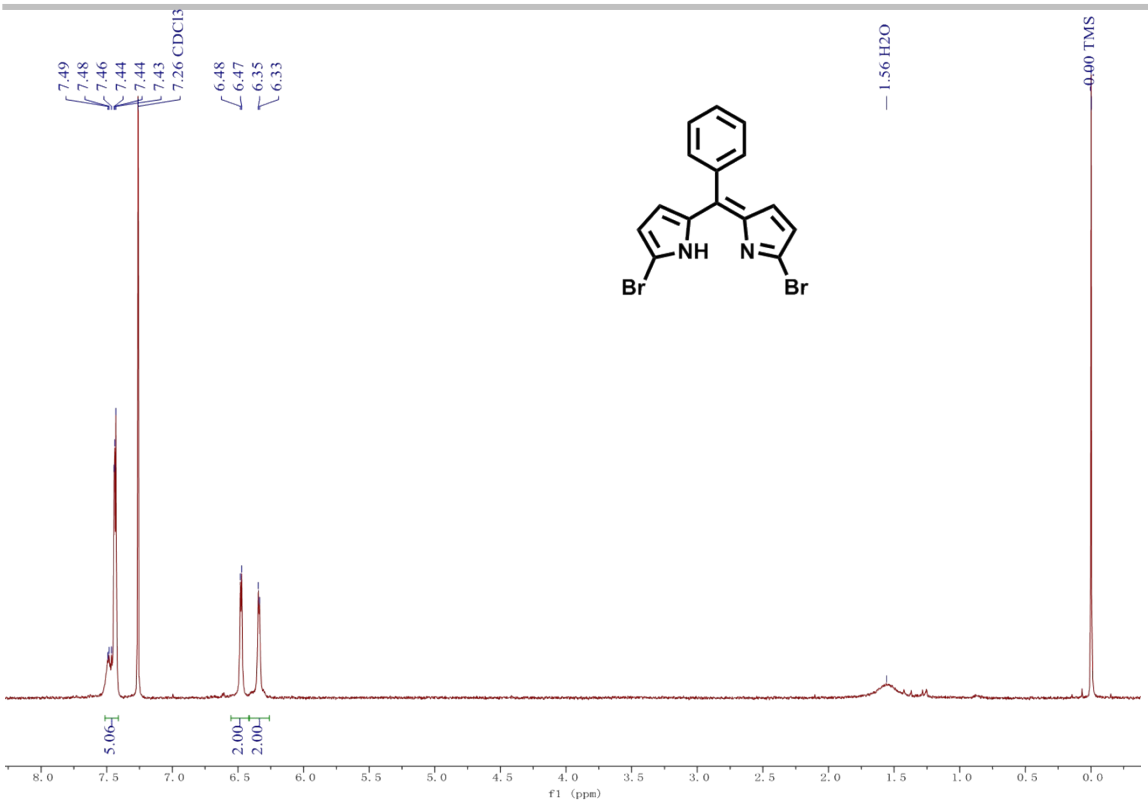

Fig. S4 ^{1}H NMR chart of 5-phenyl-α,α'-dibromodipyrrin (400 MHz, $CDCl_3$).

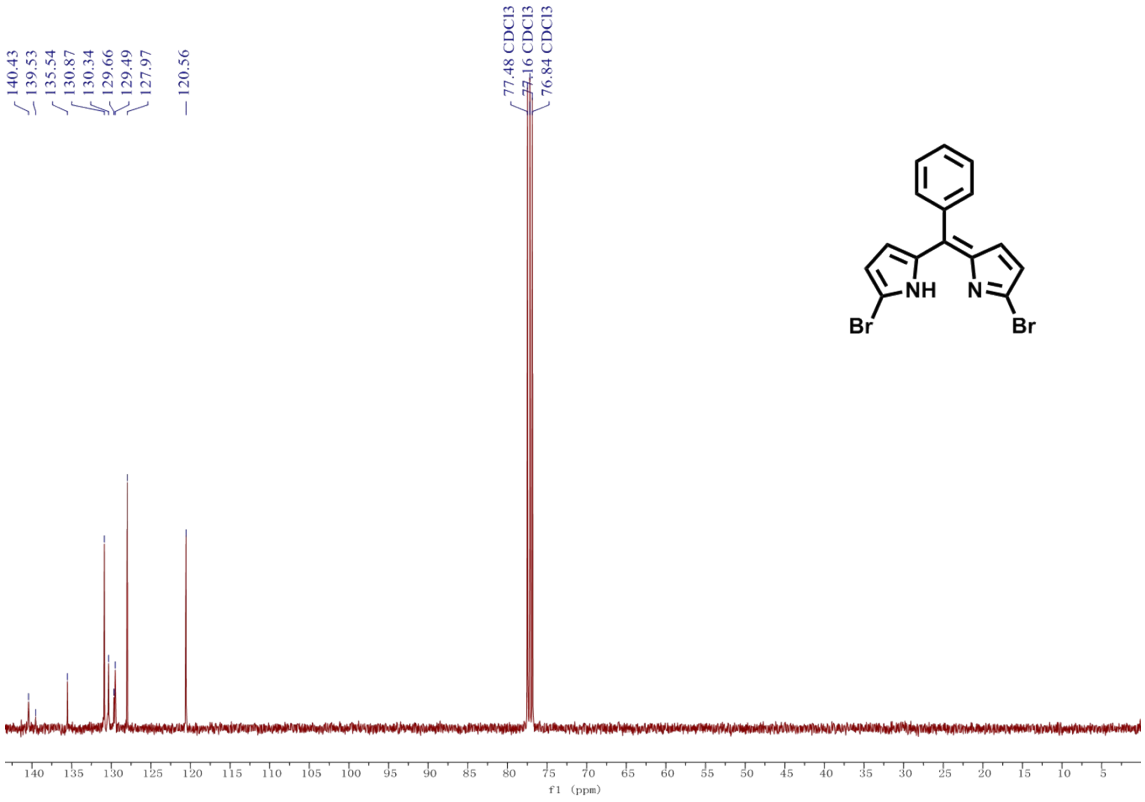

Fig. S5 $^{13}C\{^{1}H\}$ NMR chart of 5-phenyldipyrromethane (101 MHz, $CDCl_3$).

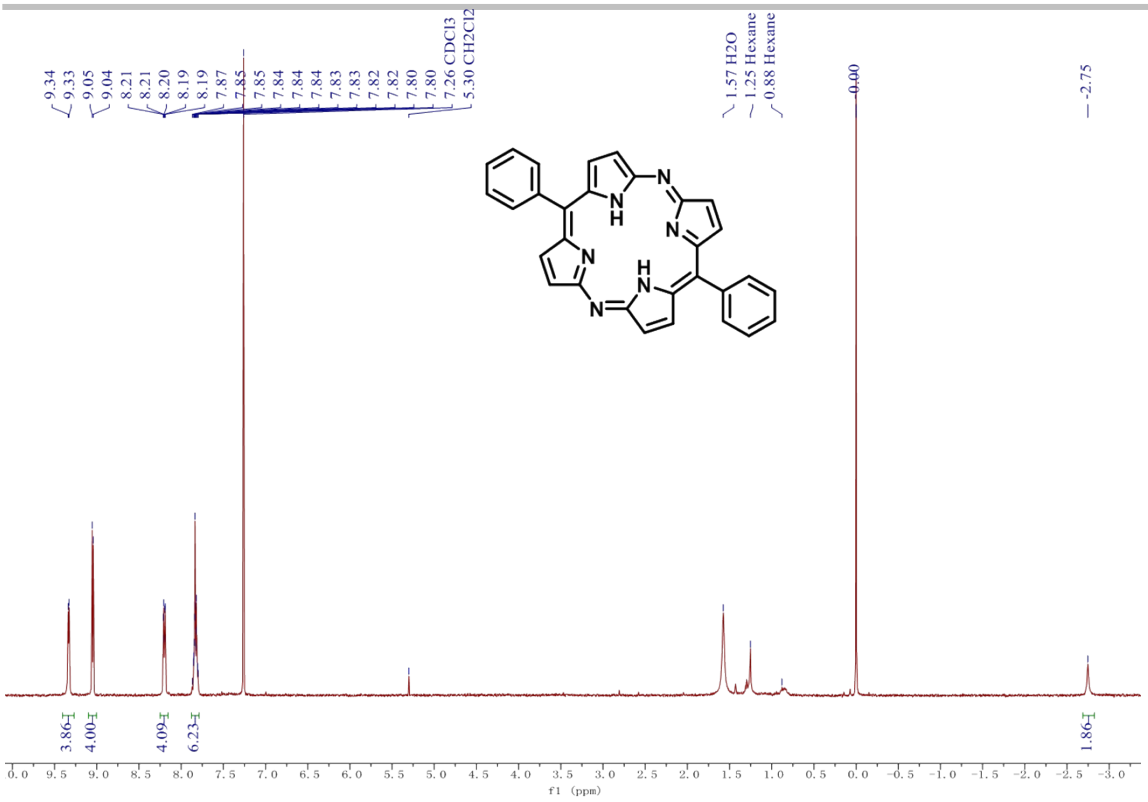

Fig. S6 ^{1}H NMR chart of 5,15-diazaporphyrin (400 MHz, $CDCl_3$).

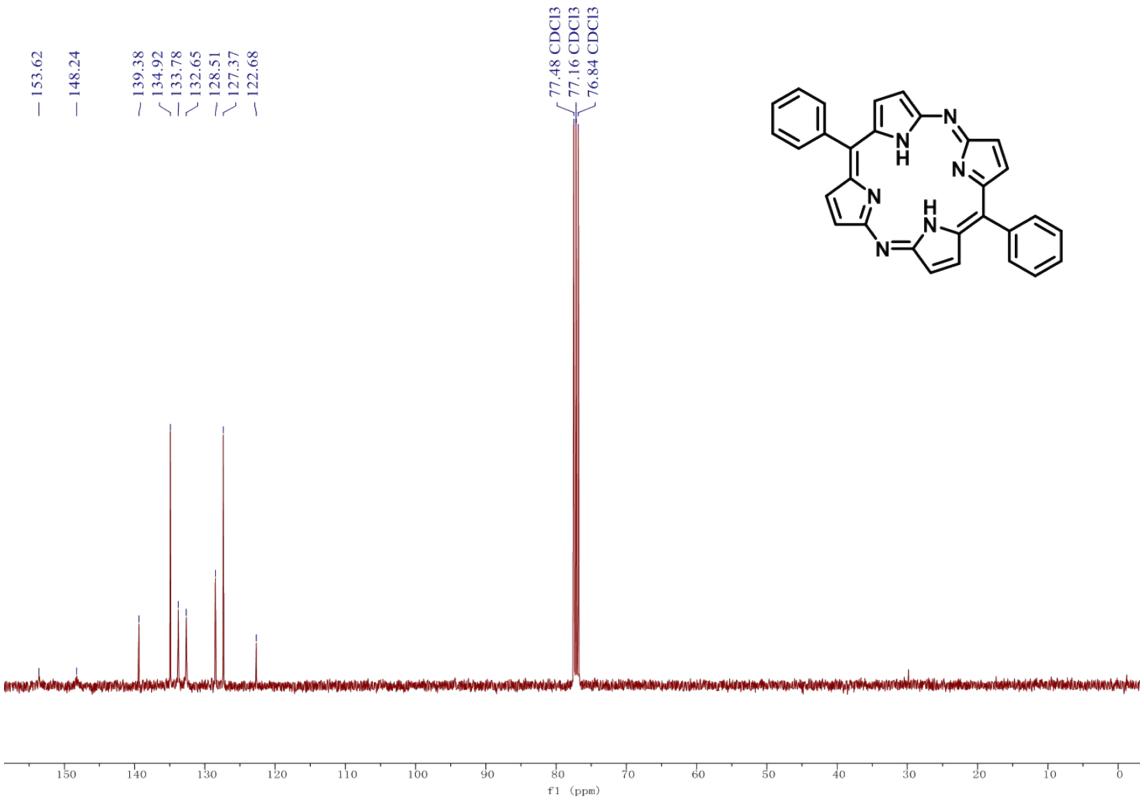

Fig. S7 $^{13}C\{^{1}H\}$ NMR chart of 5,15-diazaporphyrin (101 MHz, $CDCl_3$).

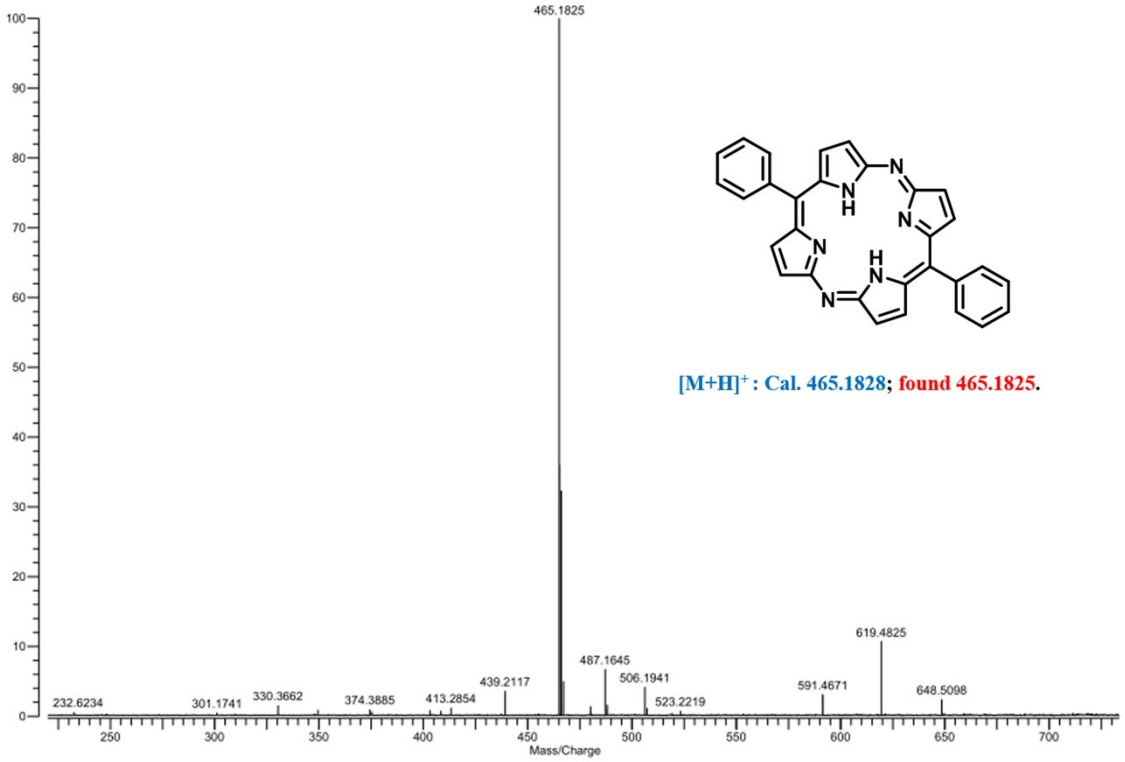

Fig. S8 ESI-HRMS chart of 5,15-diazaporphyrin.

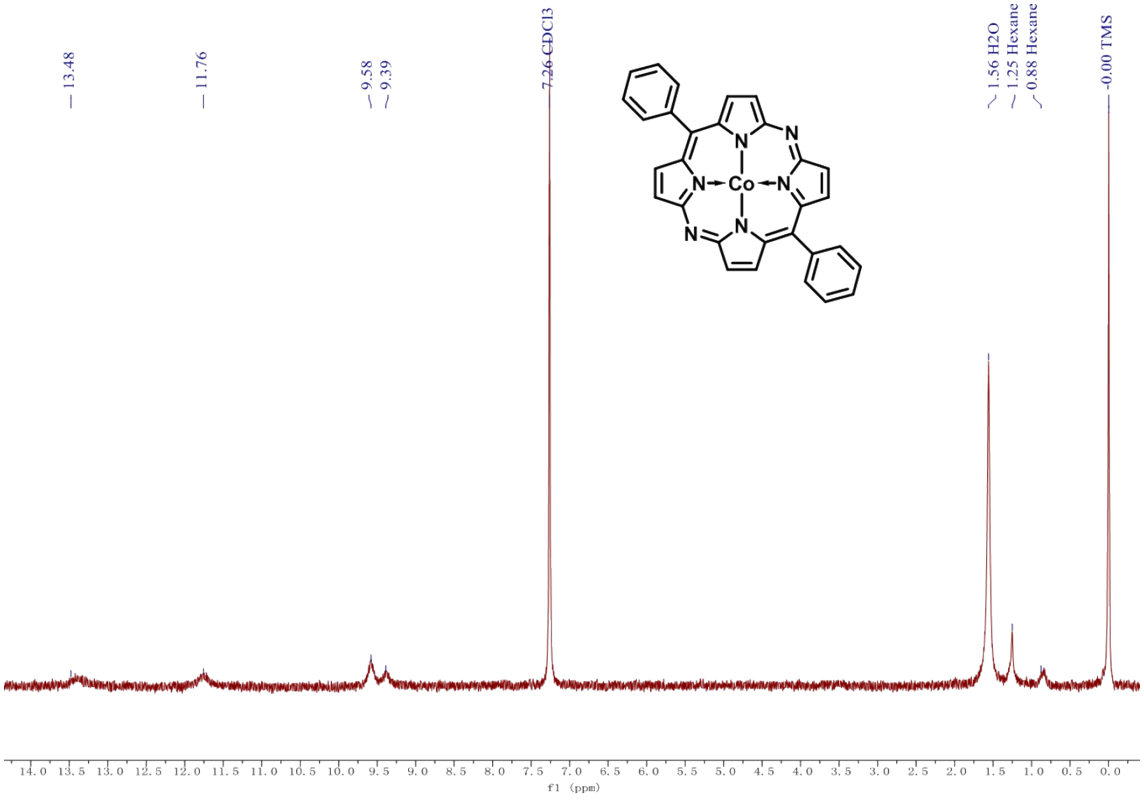

Fig. S9 ^{1}H NMR chart of Co 5,15-diazaporphyrin (400 MHz, $CDCl_3$).

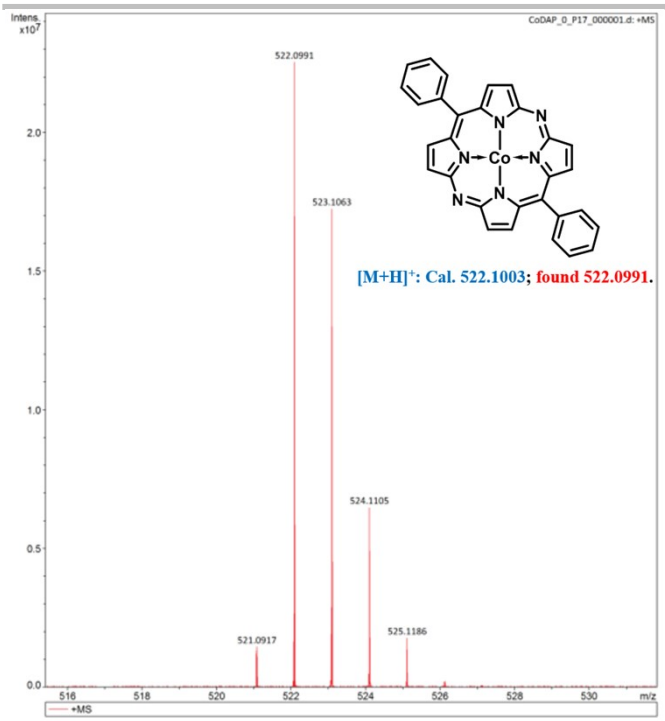

Fig. S10 MALDI-HRMS chart of Co 5,15-diazaporphyrin.

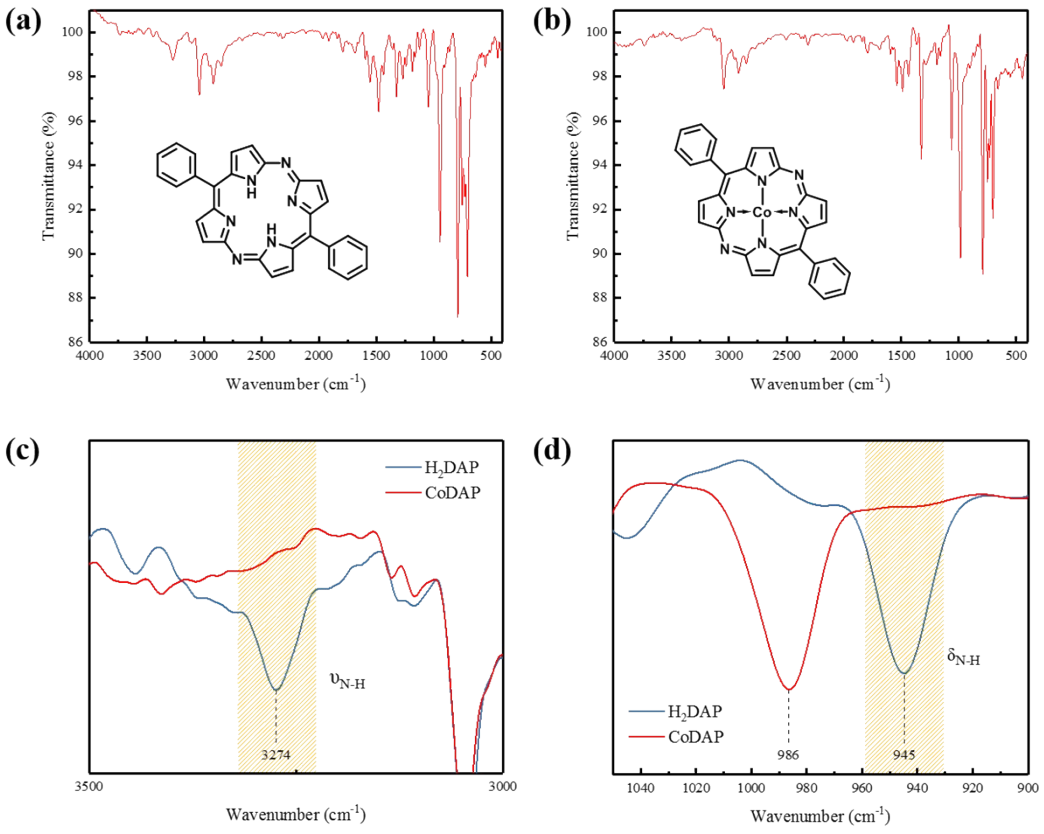

Fig. S11 FTIR charts of H_2DAP and CoDAP.

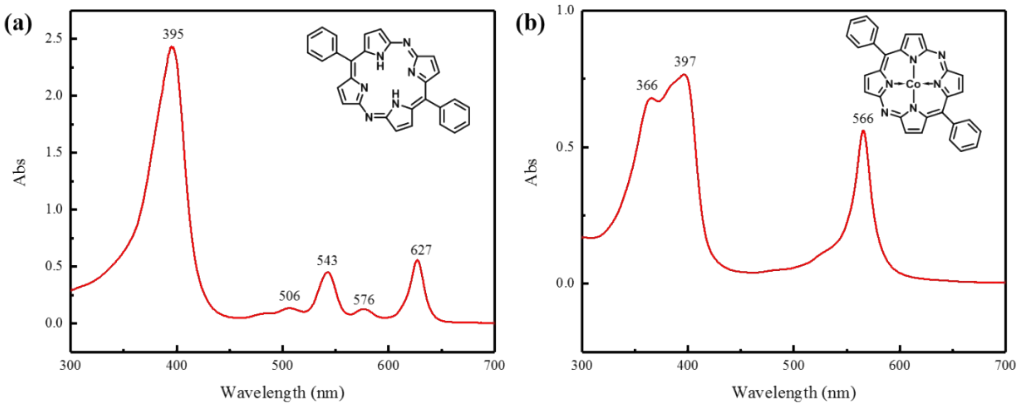

Fig. S12 UV-Vis charts of H_2DAP and CoDAP (~2*10^{-4} M in DMF).

8. Supplementary results of electrochemical measurements

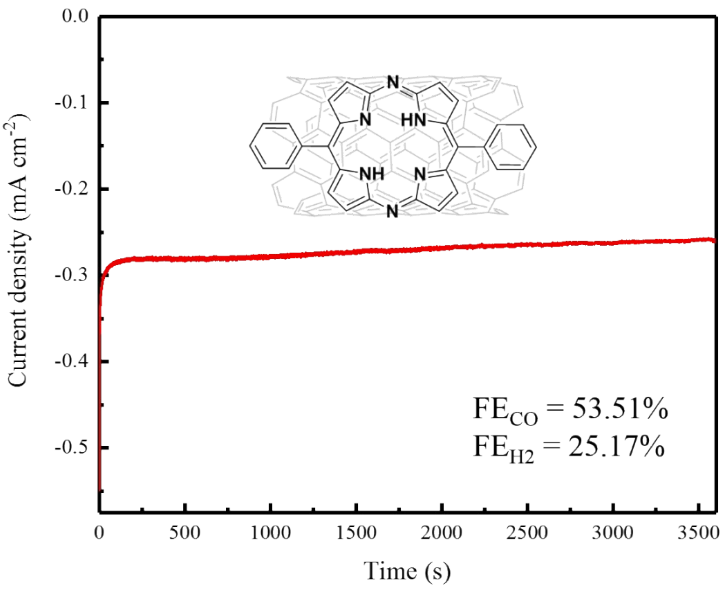

Fig. S13 Current densities of DAP/CNT during controlled potential electrolysis at -0.7 V_{RHE} in 0.1 M $KHCO_3$ under CO_2 atmosphere.

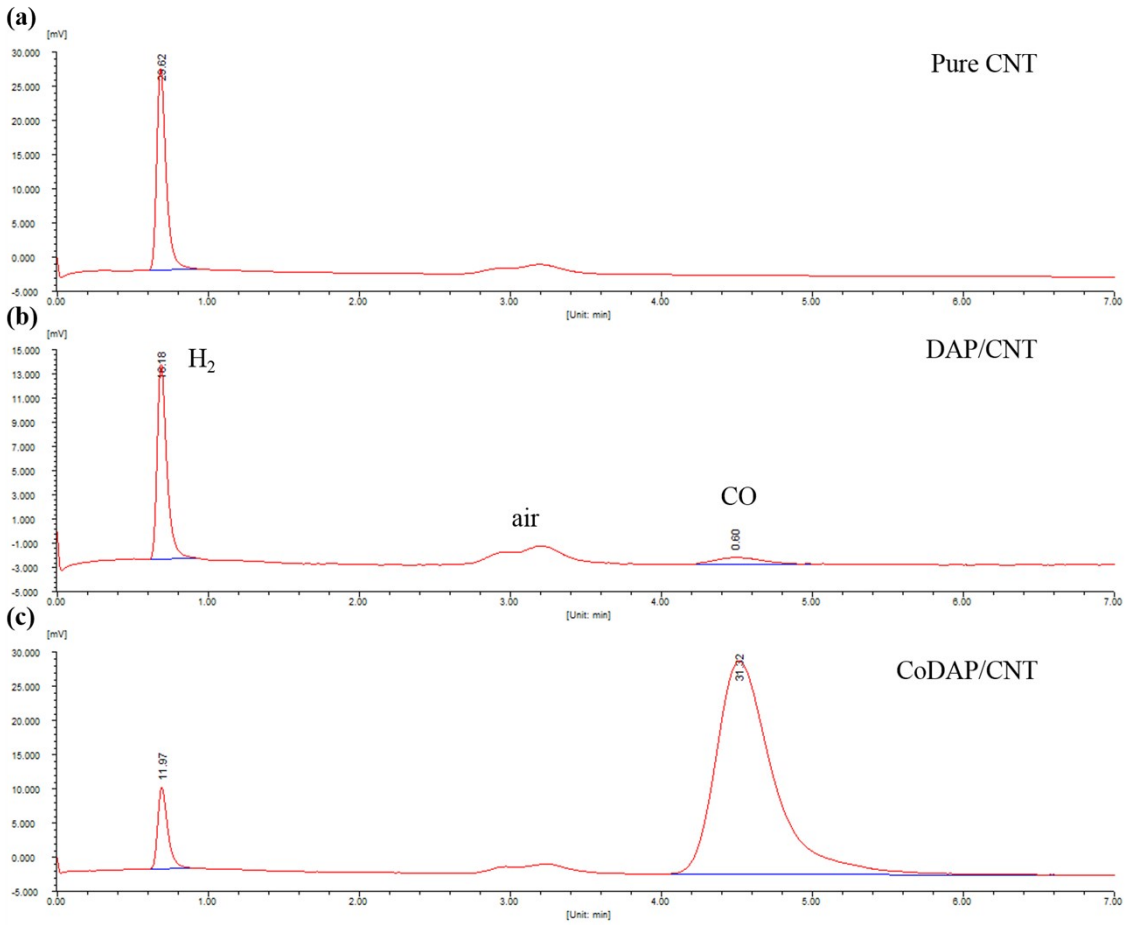

Fig. S14 Exploration of active centre for ECO_2RR. Typical gas chromatography diagrams of (a) pure CNT, (b) DAP/CNT and (c) CoDAP/CNT after electrolysis for 1 h.

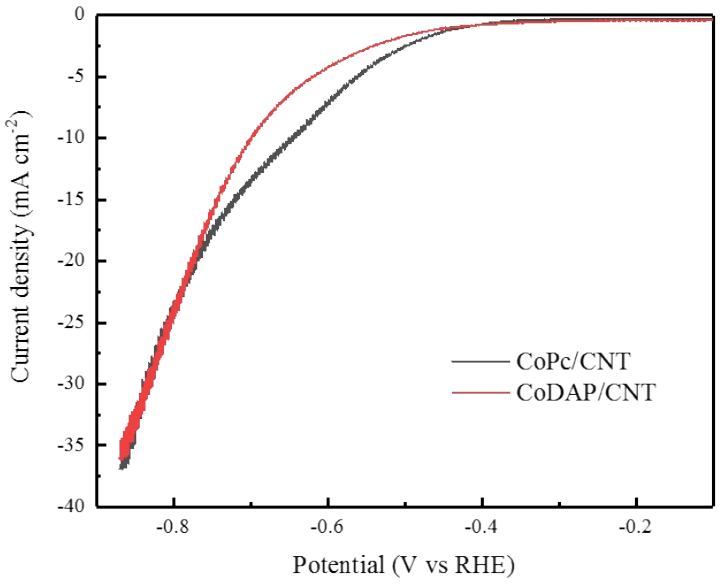

Fig. S15 LSV curves of CoDAP/CNT and CoPc/CNT under CO_2.

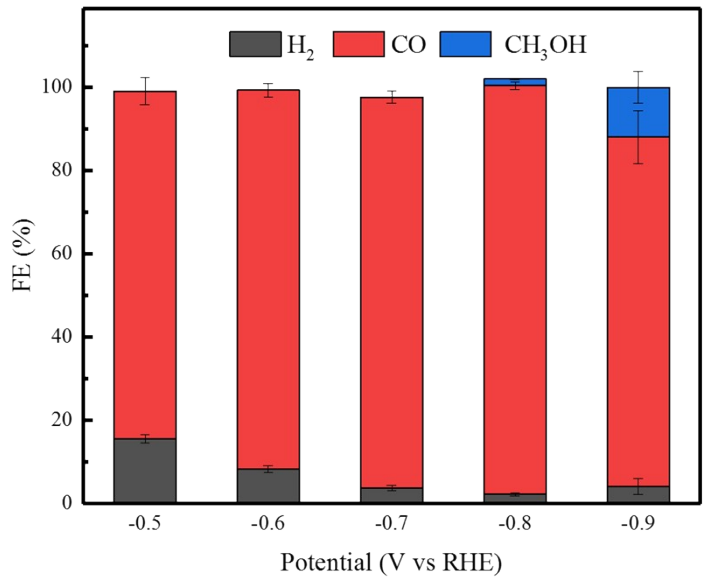

Fig. S16 FE of CoPc/CNT for each product under different potentials after 1 h of CPE under CO_2. The average values and error bars were based on three parallel experiments.

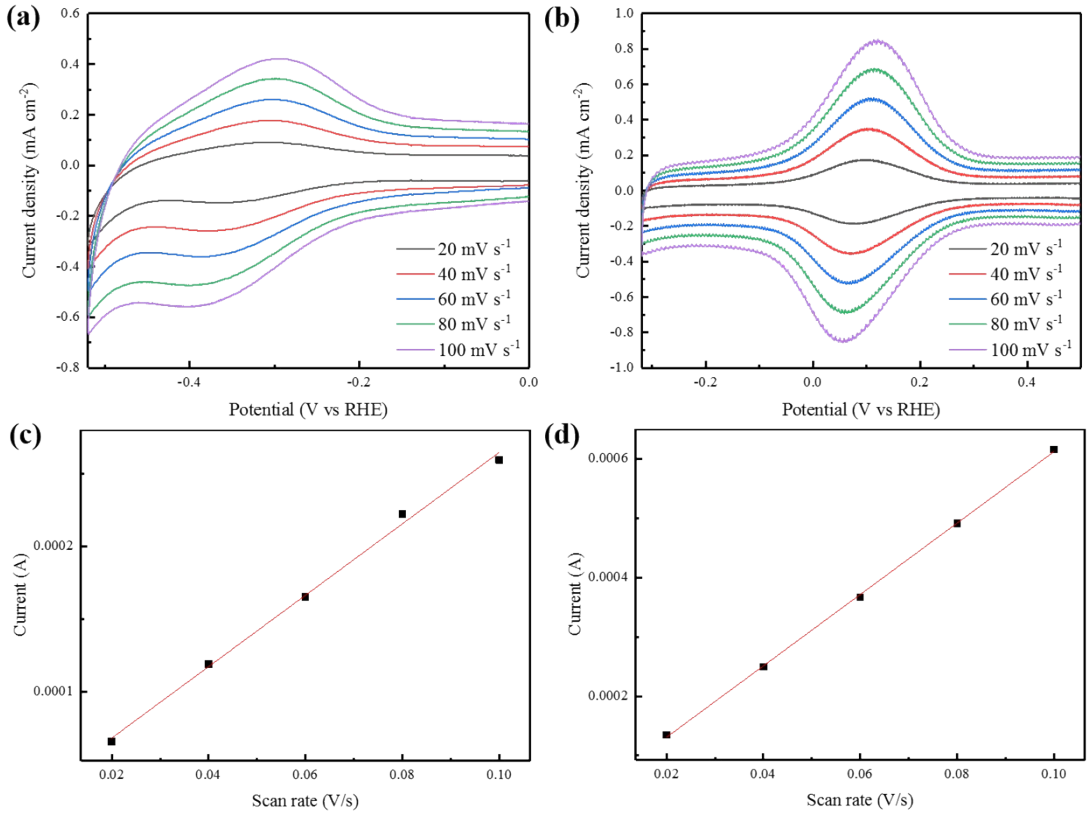

Fig. S17 Scan rate dependence from 0.02 to 0.1 V/s of the Co(II)/Co(I) redox couples for (a) CoDAP/CNT and (b) CoPc/CNT in 0.1 M pH 8.2 aqueous $KHCO_3$ solution under Ar atmosphere. Plots of Co(II)/Co(I) cathodic peak currents as a function of scan rate for (a) CoDAP/CNT and (b) CoPc/CNT.

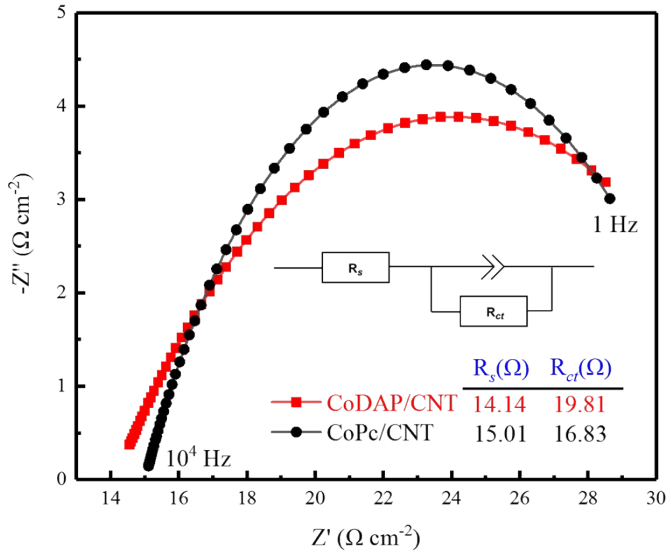

Fig. S18 EIS chart of CoDAP/CNT and CoPc/CNT at -0.7 V_{RHE} under CO_2. The inset is the equivalent circuit model.

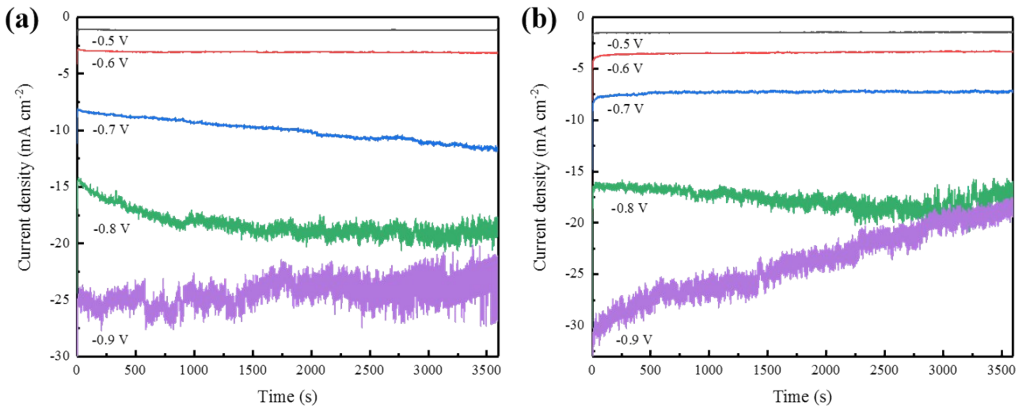

Fig. S19 Current density curves of CPE tests at different potentials for (a) CoDAP/CNT and (b) CoPc/CNT.

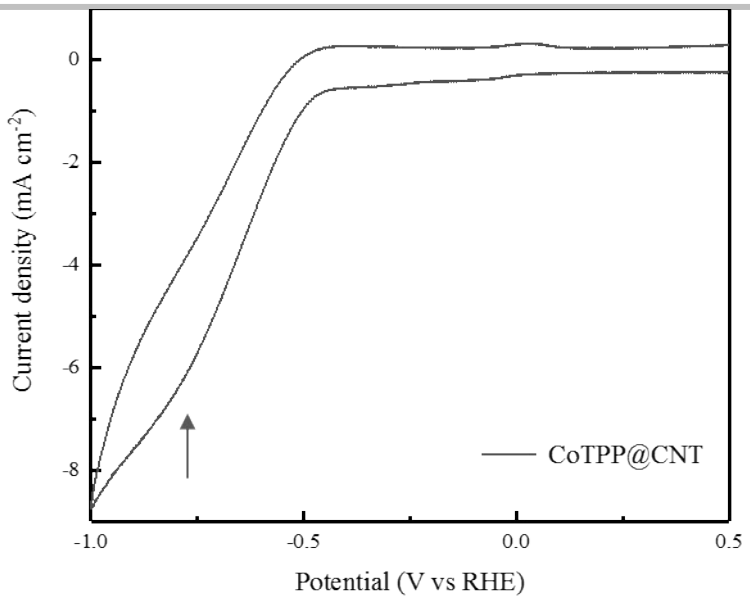

Fig. S20 CV curves of CoTPP@CNT recorded at 100 mV s^{-1} in CO_2 saturated 0.1 M $KHCO_3$. The distinct Co(II)/Co(I) reduction peaks were indicated.

9. DFT calculations of Mulliken charge distribution

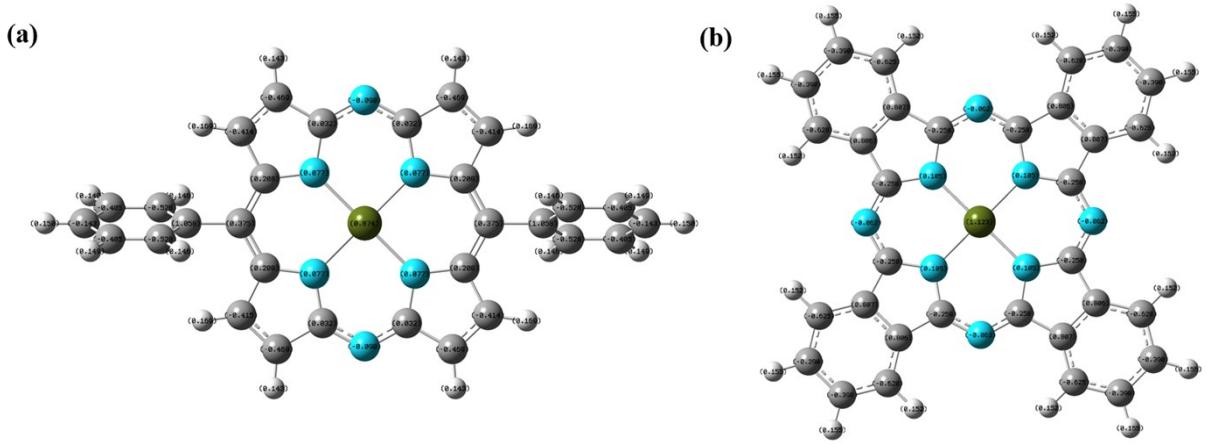

Fig. S21 Mulliken charge distribution of (a) CoDAP and (b) CoPc.

10. Electrocatalytic measurement system and CO_2 reduction products analysis

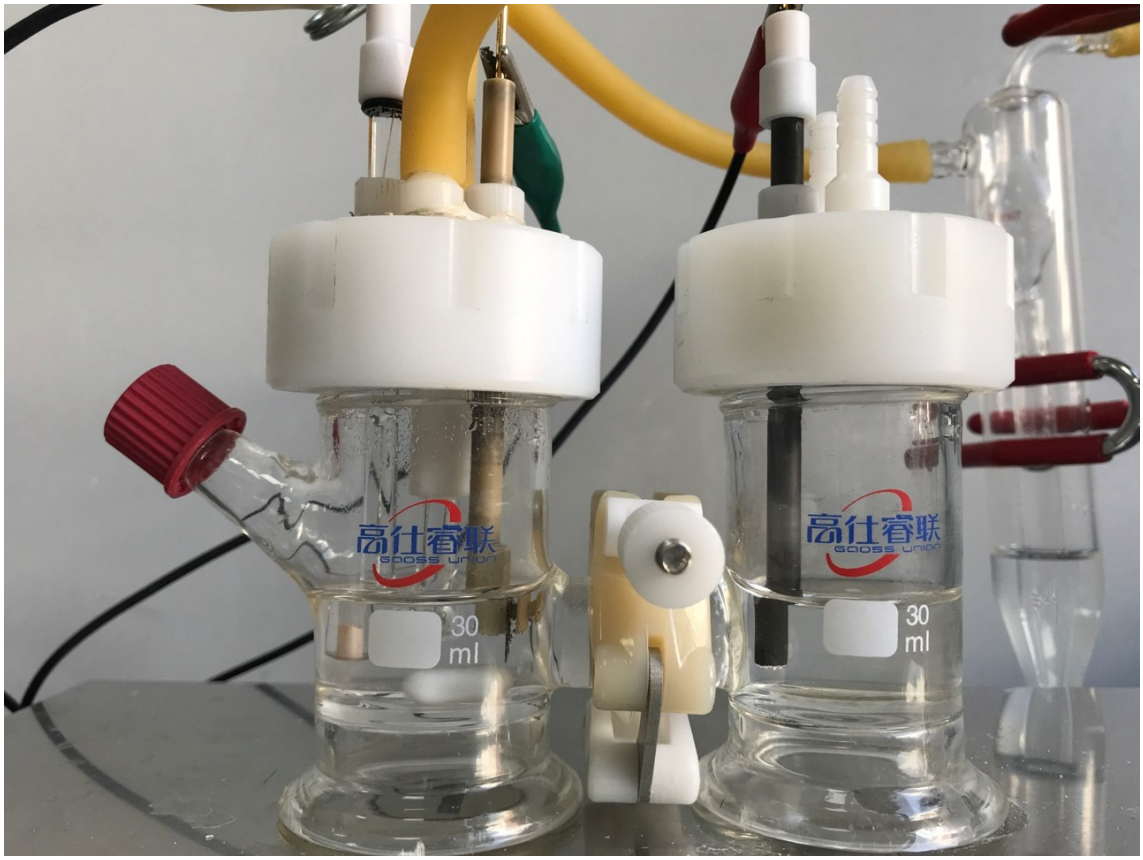

Fig. S22 Digital photograph of the electrocatalytic measurement system.

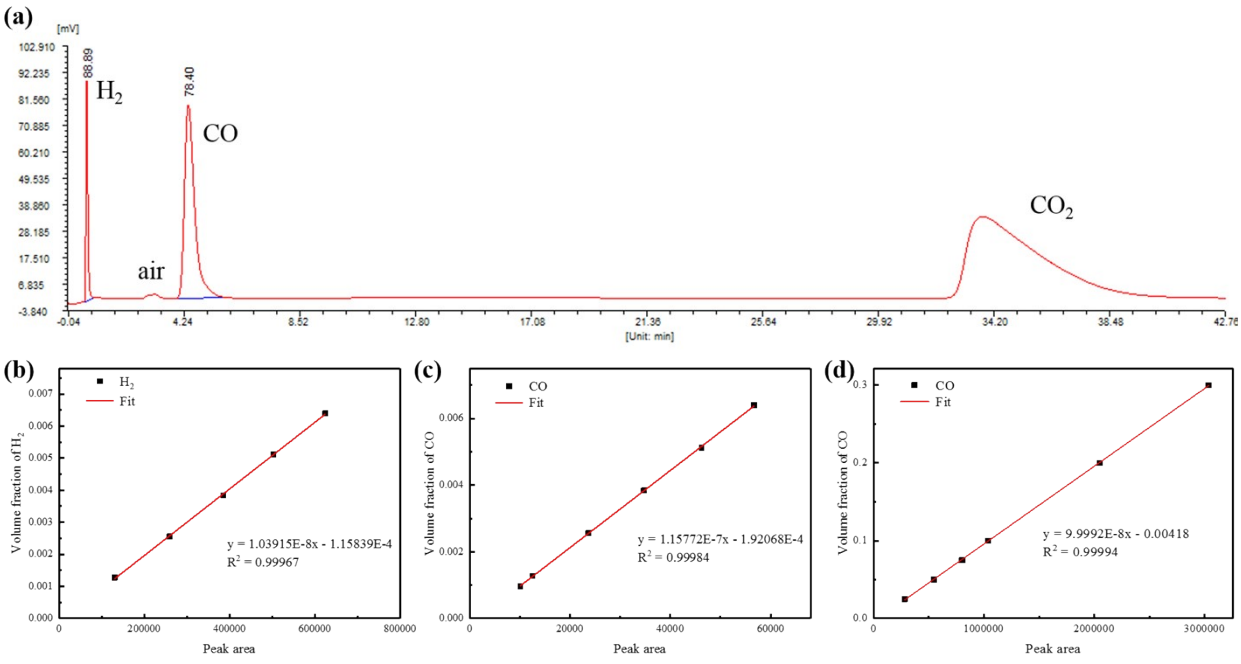

Fig. S23 (a) Gas chromatogram of the gas product. Calibration curves for (b) H_2 and (c, d) CO detected by GC-TCD.

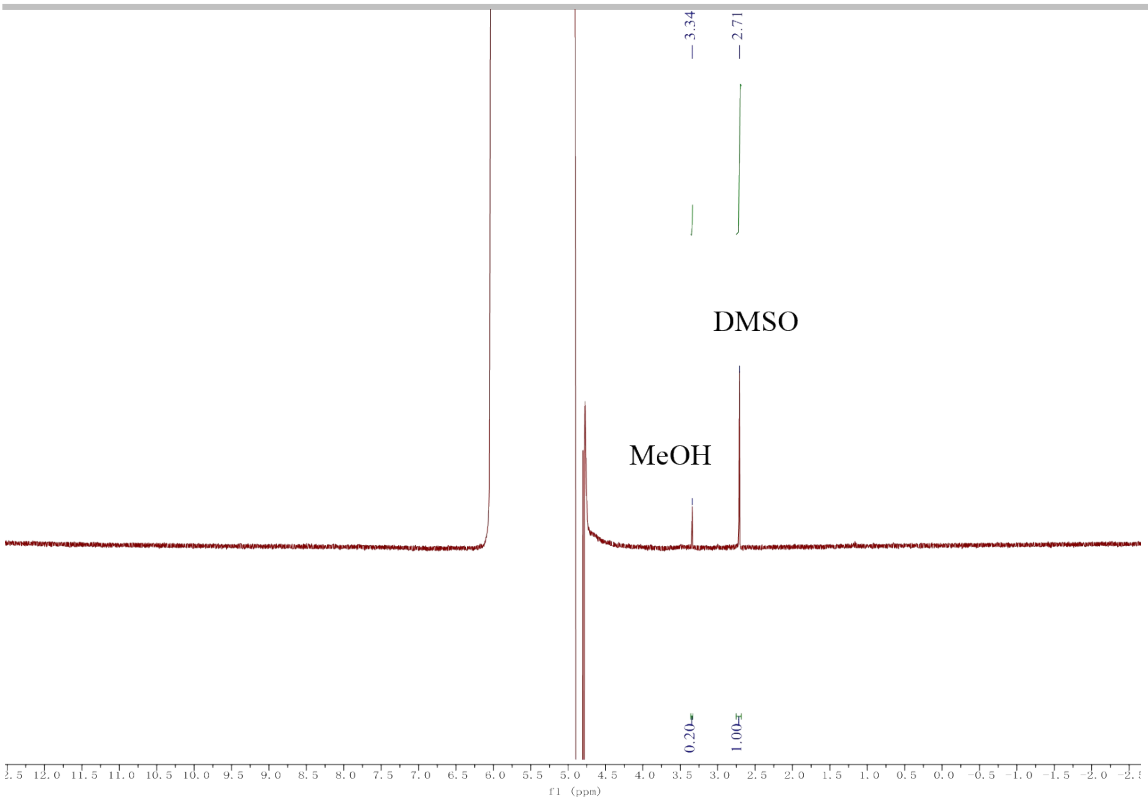

Fig. S24 ^{1}H NMR spectra of the liquid product for ECO$_2$RR (400 MHz, D$_2$O:H$_2$O = 1:9).

11. Comparison of ECO_2RR performances of cobalt porphyrinoids

Table S1 Comparison of ECO_2RR performances of cobalt porphyrinoids. Heterogeneous catalysts for the electrochemical reduction of CO_2 in this review. The full names of the acronyms for electrode materials are as following: CNT (carbon nanotubes), Py-CNT (pyridine-functionalized carbon nanotubes), CNY-OH (hydroxyl-functionalized carbon nanotubes), CB (carbon black), NrGO (N-doped reduced graphene oxide), P4VP (poly-4-vinylpyridine), GC (glassy carbon), CP (carbon paper), CC (carbon cloth). * represents the electroactive concentration. # represents $eTOF_{CO}$.

Catalysts	Support	Working electrode	FE_{CO} (%)	Potential	j_{total} (mA cm^{-2})	Loading concentration (nmol cm^{-2})	TOF_{CO} (s^{-1})	Electrolyte	Stability (h)	Ref.
CoDAP	CNT	CP	99.0	-0.7 vs. RHE	10.0	23.3 2.6*	2.4 19.6#	0.1 M $KHCO_3$	10 h	This work
CoDAP	CNT	CP	~100	-0.8 vs. RHE	17.9	23.3 2.6*	4.0 35.82#	0.1 M $KHCO_3$	-	This work
CoPc	CNT	CP	98.2	-0.8 vs. RHE	17.4	35.2 6.4*	2.5 13.82#	0.1 M $KHCO_3$	-	This work
CoTPP	CNT	GC	91	-0.753 vs. RHE	3.2	170	0.078	0.5 M $KHCO_3$	4 h	[14]
CoPc	CNT	CP	92	-0.63 vs. RHE	~10.0	~17.6	2.7	0.1 M $KHCO_3$	10 h	[15]
CoPc-CN	CNT	CP	98	-0.63 vs. RHE	~15.0	~18.3	4.1	0.1 M $KHCO_3$	-	[15]
Co(II)CPY	CNT	CP	~96	-0.7 vs. RHE	~10.7	59.3	9.59	0.1 M $KHCO_3$	11.33 h	[16]
CoIICNPY	Py-CNT	CP	~98	-0.75 vs. RHE	~7.5	~57.7	0.82	0.1 M $KHCO_3$	20 h	[17]
CoPc2	CNT	CP	93	-0.676 vs. RHE	~19.5	14.4	6.8	0.5 M $NaHCO_3$	10 h	[18]
CoTMAPc	CNT	CP	~98	-0.62 vs. RHE	~14	~7	~13	0.5 M $KHCO_3$	12 h	[19]
CoPPCl	CNT-OH	CP	98.3	-0.6 vs. RHE	25.1	~96.8	1.37	0.5 M $NaHCO_3$	12 h	[20]
CoPc	Py-CNT	CP	98.4	-0.63 vs. RHE	5.5	5	4.86	0.2 M $NaHCO_3$	12 h	[21]
CoTPP	-	CC	67	-1.05 vs. NHE	-	0.69*	8.3#	0.5 M $KHCO_3$	8 h	[22]
CoPcP	*meso* TiO_2	Ti foil	85	-1.09 vs. SHE	1.5	27 ± 1*	0.27#	0.5 M $KHCO_3$	2 h	[23]
CoPcS4	PPy	CC	>95	-0.9 vs. RHE	~3.2	~50	830 TON_{CO}	0.1 M $KHCO_3$	10 h	[24]
CoTMAP	NrGO	CP	~90	-0.8 vs. RHE	~3.5	-	-	0.5 M $NaHCO_3$	0.5	[25]
CoPc	P4VP	edge-plane graphite disc electrode	89	-0.73 vs. RHE	2.0	1.3	4.8	0.1 M NaH_2PO_4, pH=5 (1 M NaOH)	2 h	[26]

References

1. J. K. Laha, S. Dhanalekshmi, M. Taniguchi, A. Ambroise and J. S. Lindsey, *Org. Process Res. Dev.*, 2003, **7**, 799-812.
2. H. Omori, S. Hiroto and H. Shinokubo, *Org. Lett.*, 2016, **18**, 2978-2981.
3. H. Uehara, Y. Shisaka, T. Nishimura, H. Sugimoto, Y. Shiro, Y. Miyake, H. Shinokubo, Y. Watanabe and O. Shoji, *Angew. Chem. Int. Ed.*, 2017, **56**, 15279-15283.
4. M. Nishijo, S. Mori, T. Nishimura, H. Shinokubo and Y. Miyake, *Chem. Asian J.*, 2022, **17**, e202200305.
5. X. Zhang, Z. Wu, X. Zhang, L. Li, Y. Li, H. Xu, X. Li, X. Yu, Z. Zhang, Y. Liang and H. Wang, *Nat. Commun.*, 2017, **8**, 14675.
6. M. Loipersberger, D. G. A. Cabral, D. B. K. Chu and M. Head-Gordon, *J. Am. Chem. Soc.*, 2021, **143**, 744-763.
7. L. Goerigk, A. Hansen, C. Bauer, S. Ehrlich, A. Najibi and S. Grimme, *Phys. Chem. Chem. Phys.*, 2017, **19**, 32184-32215.
8. A. De Riccardis, M. Lee, R. V. Kazantsev, A. J. Garza, G. Zeng, D. M. Larson, E. L. Clark, P. Lobaccaro, P. W. W. Burroughs, E. Bloise, J. W. Ager, A. T. Bell, M. Head-Gordon, G. Mele and F. M. Toma, *ACS Appl. Mater. Interfaces*, 2020, **12**, 5251-5258.
9. G. Kresse and J. Furthmüller, *Comput. Mater. Sci.*, 1996, **6**, 15-50.
10. G. Kresse and J. Furthmüller, *Phys. Rev. B*, 1996, **54**, 11169-11186.
11. J. P. Perdew, K. Burke and M. Ernzerhof, *Phys. Rev. Lett.*, 1996, **77**, 3865-3868.
12. G. Kresse and D. Joubert, *Phys. Rev. B*, 1999, **59**, 1758-1775.
13. P. E. Blöchl, *Phys. Rev. B*, 1994, **50**, 17953-17979.
14. X. M. Hu, M. H. Ronne, S. U. Pedersen, T. Skrydstrup and K. Daasbjerg, *Angew. Chem. Int. Ed. Engl.*, 2017, **56**, 6468-6472.
15. X. Zhang, Z. Wu, X. Zhang, L. Li, Y. Li, H. Xu, X. Li, X. Yu, Z. Zhang, Y. Liang and H. Wang, *Nat. Commun.*, 2017, **8**, 14675.
16. L. Sun, Z. Huang, V. Reddu, T. Su, A. C. Fisher and X. Wang, *Angew. Chem. Int. Ed. Engl.*, 2020, **59**, 17104-17109.
17. L. Sun, V. Reddu, T. Su, X. Chen, T. Wu, W. Dai, A. C. Fisher and X. Wang, *Small Struct.*, 2021, **2**, 2100093.
18. M. Wang, K. Torbensen, D. Salvatore, S. Ren, D. Joulié, F. Dumoulin, D. Mendoza, B. Lassalle-Kaiser, U. Işci, C. P. Berlinguette and M. Robert, *Nat. Commun.*, 2019, **10**, 3602.
19. J. Su, J.-J. Zhang, J. Chen, Y. Song, L. Huang, M. Zhu, B. I. Yakobson, B. Z. Tang and R. Ye, *Energy Environ. Sci.*, 2021, **14**, 483-492.
20. M. Zhu, J. Chen, L. Huang, R. Ye, J. Xu and Y. F. Han, *Angew. Chem. Int. Ed. Engl.*, 2019, **58**, 6595-6599.
21. M. Zhu, J. Chen, R. Guo, J. Xu, X. Fang and Y.-F. Han, *Appl. Catal., B*, 2019, **251**, 112-118.
22. A. N. Marianov and Y. Jiang, *Appl. Catal., B*, 2019, **244**, 881-888.
23. S. Roy, M. Miller, J. Warnan, J. J. Leung, C. D. Sahm and E. Reisner, *ACS Catal.*, 2021, **11**, 1868-1876.
24. J. M. Chen, W. J. Xie, Z. W. Yang and L. N. He, *ChemSusChem*, 2022, **15**, e202201455.
25. M. Zhu, C. Cao, J. Chen, Y. Sun, R. Ye, J. Xu and Y.-F. Han, *ACS Appl. Energy Mater.*, 2019, **2**, 2435-2440.
26. W. W. Kramer and C. C. L. McCrory, *Chem. Sci.*, 2016, **7**, 2506-2515.